J Appl Electrochem (2009) 39:1443–1449
DOI 10.1007/s10800-009-9823-4

ORIGINAL PAPER

Enhancement of electrocatalytic O_2 reduction on carbon nanotube-supported Pt alloys nanoparticles in gas diffusion electrodes

Ahmad Nozad Golikand · Elaheh Lohrasbi · Mohammad Ghannadi Maragheh · Mehdi Asgari

Received: 25 June 2008 / Accepted: 29 January 2009 / Published online: 19 February 2009

Abstract The use of Pt binary and ternary alloys prepared by alloying of Pt with transition metals, as catalysts for fabricating of gas diffusion electrodes (GDEs) is reported. Electrocatalytic properties of oxygen reduction reaction (ORR) were evaluated by cyclic voltammetry, electrochemical impedance spectroscopy, polarization experiments and chronoamperometry. The morphology of the GDEs and elemental compositions of the Pt alloys were characterized by X-ray diffraction (XRD) analysis and inductively coupled plasma atomic emission spectroscopy (ICP-AES) system. The results indicate that the introduction of Pd and Cd as transition metals in Pt alloys provides fast ORR kinetics. The performance of GDEs with Pt–Pd alloy surfaces for ORR was also studied as a function of overall composition and surface atomic distribution of Pt alloys. The results also show that alloying of Pt with transition metals and various amounts of Pt and Pd in the binary catalysts has a large effect on the performance of GDEs for ORR.

Keywords Platinum · Alloy · Oxygen reduction reaction · Gas diffusion electrode

1 Introduction

Polymer-electrolyte fuel cells (PEFCs) have attracted great attention due to their high power density, low-temperature operation and environmentally friendly technology. Nano-sized platinum catalysts are used both in the cathode and anode of the PEFCs. A high dispersion is required to enhance catalytic activity and reduce the amount of expensive precious metals used. The wide variety of pore structures and chemical functional groups on the surface of carbon supports affects the dispersion of Pt nanoparticles [1]. Among the various carbon supports, carbon nanotubes (CNTs) are very attractive as electrocatalyst supports, because they have unique physicochemical characteristics such as good intrinsic conductivity, a pore structure without micro pores, durability under corrosive conditions and mechanical toughness.

In order to reduce cathode activation losses due to the comparably sluggish kinetics of the oxygen reduction reaction, more active catalysts must be used [2–4]. One way to improve cathode performance is to use supported Pt catalysts that have higher surface area and lower platinum loading [5–10]. Further improvement in the reduction of cathode activation potential, and at the same time to lower its price, can be achieved by using Pt-based alloys with transition metals. In the last decades, oxygen reduction on platinum surfaces and especially on platinum alloys has captured the attention of both experimental [11–18] and theoretical [19–24] researchers due to its importance in fuel cells and other energy conversion systems. Despite the interest, there are still unresolved issues stemming from slow kinetics of the reactions and also from the incomplete understanding of its mechanism. Alloy catalysts have been proposed and tested with various degrees of success, attributed to the changes in their electronic structure with respect to that of Pt and to the changes in their physical structure (metal–metal distances and coordination numbers). It has been demonstrated that the use of alloys such as Pt–Fe, Pt–Ni, Pt–Co and Pt–Cr leads to an enhancement in the activity of oxygen reduction on the cathode of the fuel cells compared with pure platinum. Recent

A. N. Golikand (✉) · M. G. Maragheh · M. Asgari
Chemistry Department, NSTRI, Tehran, Iran
e-mail: ahmadnozadgolikand@yahoo.com

A. N. Golikand · E. Lohrasbi
Corrosion Laboratory, School of Materials, NSTRI, Tehran, Iran

experimental work [13–15, 18, 24–28] has tested the use of bimetallic Pt alloys as oxygen reduction catalysts. Wang et al. studied the reaction thermodynamics for the direct four electron reduction through evaluating the Gibbs free energy change for each step on a group of transition metal atoms [20]. This analysis indicated that it is possible to separate the effect of the first reduction step from those of the last three steps, which may be considered coupled. Wang et al. and Sidik et al. assumed that the oxygen molecule does not dissociate before the first electron and proton transfer and that the product for this step is OOH, which dissociates on the surface as suggested [20, 21]. Wang et al. studied the change in reaction energy (at 0 K) for the direct four electron reduction through evaluating ΔE1 for the first electron reduction step on a given metal site, M, as:

$$O_2 + M + H^+ + e^- \rightarrow M{-}OOH \quad (1)$$

Followed by ΔE2 for the reaction:

$$M{-}OH + M{-}O + 3H^+ + 3e^- \rightarrow 2M + 2H_2O \quad (2)$$

This combines the last three electrons and proton transfers, representing the successive reductions of the adsorbed hydroxyl and atomic oxygen—resulting from the dissociation of the OOH intermediate—to water molecules [29]. Calvo et al. also proposed [30] that a good ORR catalyst could be designed as the combination of a metal that adsorbs OOH more strongly than Pt, and a second metal able to bind OH and O less strongly than Pt, thus favoring O and OH reduction to water. Many studies have used Eqs. 1 and 2 to evaluate the performance of various Pt–Pd combinations [18, 23, 24, 31, 32].

The purpose of this study is to improve the catalytic activity of platinum, by alloying it with transition metals, for the oxygen reduction reaction at cathode sites; and to investigate the electrochemical and electrocatalytic characteristics of binary and ternary alloys in GDEs. Pt binary and ternary alloy catalysts were prepared with Pd and Cd. The alloy catalysts were characterized by X-ray diffraction and ICP-AES. The alloy catalysts were supported on SWCNTs, used in the catalyst layer of GDEs, and characterized by various electrochemical techniques. The present work focuses on the preparation of Pt alloy catalysts with high total loading (50 wt%).

2 Experimental work

2.1 Surface modification of SWCNTs

The surfaces of commercial SWCNTs (Aldrich) were functionalized with carboxyl functional groups. For this purpose, commercial SWCNTs and concentrated nitric acid were refluxed at 140 °C for 7 h. They were then washed well with deionized water and dried to produce a modified catalyst.

2.2 Electrocatalyst preparation

To support Pt nanoparticles on SWCNTs, the well-known impregnation method followed by liquid-phase borohydride was adopted. A mixture of modified SWCNTs and H_2PtCl_6 (Aldrich) was suspended by sonication in 40 mL of deionized water. Subsequently, Pt nanoparticles were reduced and supported on the SWCNTs by $NaBH_4$ (Kanto Chemical) as the reducing agent, simultaneously, and washed with deionized water several times. The filtrate was collected to determine the exact loading by measuring the Pt residue. After drying, the Pt nanoparticles supported on the SWCNTs were obtained were then dispersed in 25 mL of de-ionized water, and ultrasonically stirred for 10 min. Appropriate amounts of 0.1 M solutions of the transition metal salts [$PdCl_2$ (Merck) or $CdCl_2$ (Merck)] were added to this suspension. The Pd or Cd precursors were reduced and supported on the SWCNTs by $NaBH_4$ as the reducing agent, and washed with deionized water several times. With the aim of studying the effect of the composition on performance of electrodes with Pt–Pd catalysts, which exhibited better performance than others, Pt–Pd alloys were prepared with different compositions (75:25, 50:50 and 25:75 atomic ratios). To study the effect of the order of deposition of Pt and Pd on SWCNTs, a Pd–Pt catalyst was prepared by deposition of Pt onto the supported Pd particles. It is to be noted that we had already prepared Pt–Pd catalyst by deposition of Pd onto the supported Pt particles. The atomic ratio of Pd and Pt in Pd–Pt alloy was adjusted to 25:75. The Cd in Pt–Cd alloy was adjusted to 75:25, and for Pt–Pd–Cd alloy it was adjusted to 60:20:20. The obtained catalysts were characterized by recording the powders X-ray diffraction (XRD) pattern on a Philips PW1800 X-ray diffractometer, using Cu Kα radiation operating at 40 kV and 30 mA. The analysis of the atomic composition of the catalysts was performed with an IRIS advantage inductively coupled plasma atomic emission spectroscopy (ICP-AES) system (Varian Austria).

2.3 Fabrication of gas diffusion electrode and electrochemical measurements

Porous GDE was constructed according to a previously described procedure [15]. To prepare the PTFE-bonded porous gas diffusion layer (GDL), a 70% commercially available carbon Vulcan (XC-72R from ElectroChem Inc.) and 30% PTFE (from ElectroChem Inc.) emulsion were used and painted onto a carbon paper TGP-H-0120 (Toray). The resulting composite structure was dried in air at 80–90 °C for 1 h, followed by thermal treatment at

250 °C for 30 min to remove the dispersion agents contained in the PTFE, and finally sintered in air at 340 °C for 15 min. The PTFE is an effective binder and impacts hydrophobicity to the gas diffusion regime of the electrode. To prepare the catalyst layer, a mixture comprised of a homogeneous suspension of Nafion solution (5 wt% from Aldrich), one of the as-prepared catalysts and isopropanol (Merck) as solvent were homogenized using a sonicator (Misonix Model S-3000) for 20 min. The prepared ink was painted on GDL, and the resulting composite structure was dried in air at 25 °C for 1 h, and finally sintered in air at 140 °C (the glass transition temperature of Nafion) for 45 min. Nafion and Pt loadings were 1 and 0.5 mg cm^{-2} in the GDEs, respectively. The reduction of oxygen was investigated with the porous GDE (geometric exposed area of 1.3 cm^2) in 2 M H_2SO_4 solution. The linear sweep voltammetry (LSV) measurements were carried out at 298 K in a conventional three-electrode cell with the O_2 flow rate of 50 ml min^{-1}. The cyclic voltammetry (CV) experiments were done under argon atmosphere. The GDEs were mounted on a Teflon holder, containing a high pyrolytic graphite disk as a current collector (which had arrangements for oxygen feed from the back of the electrode). A large-area platinum flat electrode was used as the counter electrode. An Ag/AgCl reference electrode was placed close to the surface of the working electrode. The electrochemical cell was connected to a potentiostat-galvanostat digital electrochemical analyzer (Radiometer Model DEA332), equipped with an IMT 102 electrochemical interface for the CV, chronoamperometry and LSV, and also to a computer controlled 302 Autolab electrochemical system (EcoChemie, Utrecht, Netherland), driven with GPES and FRA softwares (EcoChemie) for electrochemical impedance spectroscopy (EIS). In the present work, an AC potential amplitude of 5 mV in the frequency range 1 mHz to 10 kHz was applied.

3 Results and discussion

3.1 Cyclic voltammetry study (CV)

The cyclic voltammetry studies were carried out to determine the electrochemical surface area (ESA), and to elucidate the adsorption properties of Pt surface. The voltammograms of electrodes with various alloy catalysts in the catalyst layers are presented in Fig. 1, Table 1 shows the EAS calculated by Eq. 3 [33]:

$$\mathrm{EAS} = \frac{Q_{\mathrm{H}}}{[\mathrm{Pt}] \times 0.21} \tag{3}$$

where [Pt] represents the platinum loading (mg cm^{-2}) in the electrode, Q_H is the charge for hydrogen desorption

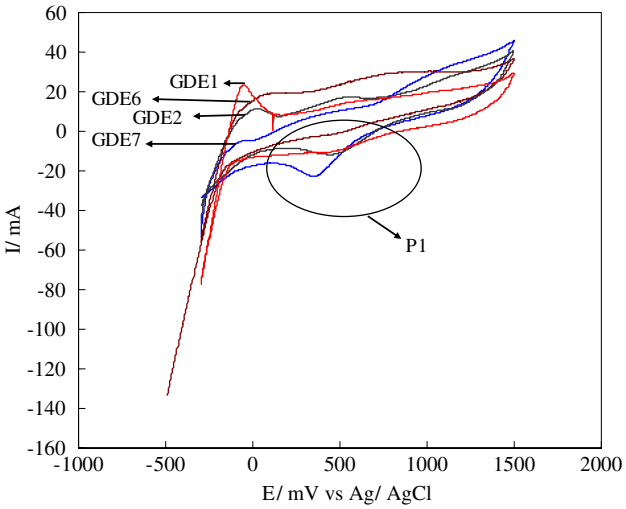

Fig. 1 Voltammograms of electrodes each with a Pt loading of 0.5 mg cm^{-2} and a Nafion loading of 1 mg cm^{-2} in the catalyst layer (scan rate 50 mV s^{-1} temperature; 25 °C)

Table 1 Q_H and EAS for the tested electrodes extracted from the voltammograms of Fig. 1

Number of GDEs	Catalyst used in GDE preparation	Q_H (mC)	EAS (m^2 g^{-1})
GDE1	Pt/CNT	73.2	69.7
GDE2	75:25 Pt–Pd/CNT	69.3	66
GDE3	50:50 Pt–Pd/CNT	51.6	49.1
GDE4	25:75 Pt–Pd/CNT	37.6	33.9
GDE5	25:75 Pd–Pt/CNT	18.7	17.8
GDE6	75:25 Pt–Cd/CNT	3.99	3.8
GDE7	60:20:20 Pt–Pd–Cd/CNT	5.78	5.5

(mC cm^{-2}) and 0.210 represents the charge required to oxidize a monolayer of H_2 on bright Pt [34–36]. As shown in Table 1, there is a marked influence of the surface composition on hydrogen adsorption capacity of the alloys. As Fig. 1 shows, GDE1 and GDE2 have larger hydrogen adsorption peaks, corresponding to higher active catalyst surface areas. Figure 1 also shows that GDE6 and GDE7 have smaller hydrogen adsorption peaks, which may be due to blocking of the Pt active sites by Cd. A single peak (p_1) during the cathodic sweep was also observed. This peak is normally assigned to the oxide reduction profile of the metals.

As can be observed in Fig. 1, the second and third metal additions has influenced the hydrogen adsorption potential, the oxide reduction potential and the charge passed due to hydrogen adsorption. Some factors that may explain this electrocatalytic performance include: (a) the ratio of low coordinated surface atoms, which increases inversely with particle size; (b) the electronic state of small metal particles; (c) the strong metal-support interaction and (d) the

synergistic effect. The loss of utilization in alloy catalyst is explained by the loss of electrochemical surface area due, in part, to the particle size and addition of transition metal ions. In the case of Pt alloys, the loss can be attributed to the decrease of Pt surface sites due to the substituted transition metals. Comparison of electrodes containing Pt–Pd, with different compositions of Pt and Pd in the catalyst layer, showed that GDE2 presented the highest active sites for hydrogen adsorption, and the excess of transition metals decreased the catalytic activities. It is also indicated that the amount of transition metals in the catalysts is one of the factors in determining the performance. As Table 1 shows, the addition of transition metals covers some Pt sites, which, in turn, decreases the available Pt sites.

3.2 Determination of kinetic parameters

In order to obtain information about the kinetic parameters of oxygen reduction reaction in the fabricated GDEs, a Tafel plot was drawn and its data were fitted by the following equations [37]:

$$E = E_0 - b\log(i) - iR \tag{4}$$

where,

$$E_0 = E_r + b\log(i_0) \tag{5}$$

In the Eqs. 4 and 5, "i_0" is the exchange current density for oxygen reduction, "b" is the Tafel slope, "E_0" is the reversible potential for the oxygen electrode reaction, and "R" represents the resistance (predominantly the ohmic resistance of the electrolyte), responsible for the linear variation of potential versus current density. The Eq. 4 is valid to the end of the linear region of the potential versus current density plot. At higher current densities, the difference of the E versus i data from Eq. 4 is due to the rapidly increasing contribution of mass-transport overpotentials. The parameters E_0, b and R were evaluated by a nonlinear least squares fitting of Eq. 4 to the experimental data. Using the R values, the iR-corrected Tafel plots ($E + iR$ versus log i) were obtained. Variations of the Tafel slope with different catalysts in the GDEs are shown in Table 2. Tafel slopes for various catalysts towards oxygen reduction lie within the range of 32–84 mV dec^{-1}. Although GDE3, GDE4 and GDE5 show slightly larger Tafel slopes than GDE1, compared to the Tafel slope values of Table 2, the Tafel slope values obtained for GDE2 is the smallest, indicating excellent performance. This is because Pd forms less stable Pd–O bonds in GDE2, which are easier to reduce comparing to Cd. It can be inferred that Cd will stabilize the Cd–O bonds, resulting in a highly negative reduction in potential that is generally too negative to be of interest in power source applications [38, 39].

Table 2 Variation of Tafel slope with different catalysts

Number of GDEs	Tafel slope (mV dec^{-1})
GDE1	53
GDE2	32
GDE3	84
GDE4	83
GDE5	71
GDE6	47
GDE7	36
GDE8	60

Comparison of the GDEs with Pt–Pd, as catalysts with different compositions of Pt and Pd in the catalyst layer, showed that GDE2 presented smaller Tafel slope. Based on this result, it is shown that GDE2 acts as a good ORR catalyst. Calvo et al. [30] showed that 3:1 Pt–Pd (in this study used in preparation of GDE2) favours the reduction of OH at the surface compared with other catalysts, allowing a weaker interaction of OH with the surface compared with other catalysts. According to their thermodynamic analysis, the best catalyst may be 3:1 Pt–Pd, which is almost as good as Pt for dissociating the O–O bond and it performs better than others for reduction of adsorbed O and OH. Their result is in good agreement with our results.

3.3 Chronoamperometry

Chronoamperometry was used to quantitatively compare the diffusivity of oxygen in the GDEs according to Jiang et al. [40]:

$$i(t) = nFA(D/\pi t)^{0.5}C^* \tag{6}$$

where, "i" is the current (mA); n is the number of electrons; "F" is the Faraday constant (96485 C mol^{-1}); "A" is the surface area of the electrode (cm^{-2}); "D" is the diffusion coefficient (cm^2 s^{-1}); "t" is the time (s), and "C^*" is the concentration of the reactant (mM). One can define $D^{0.5}C^*$ as permittivity of oxygen at GDEs. A Cottrell plot can be obtained from chronoamperometry (i versus $t^{-1/2}$) and the permittivity of oxygen can be calculated from the slope of this plot. The variation of permittivity of oxygen in the tested electrodes is shown in Fig. 2. The GDEs consist of a distribution of pores with different radii (micro and macro pores), and therefore, have different permittivity values. According to our findings, the permittivity of GDE6 is more than that of the other GDEs. This result is consistent with the ability of oxygen diffusion in the reaction layer, due to distribution of its micro and macro pores. Comparison of GDEs with Pt–Pd as catalyst, with different compositions of Pt and Pd in the catalyst layer, showed that GDE2 presented the highest permittivity

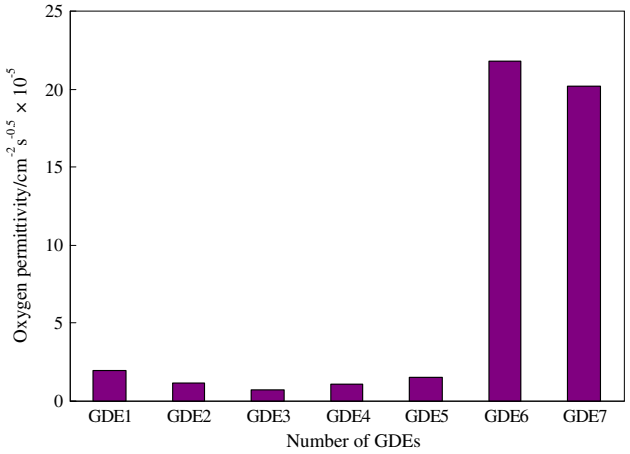

Fig. 2 Variation of permittivity of oxygen in the tested electrodes, extracted from the chronoamperometry data with different catalysts used in the preparation of GDEs

value. This result is consistent with its high porosity because of the smaller average particle size (see Sect. 3.5).

3.4 Impedance spectroscopy study

Impedance spectroscopy was used to characterize the ionic resistance; the impedance spectra were recorded at the open circuit voltage and under Argon reflux. We also assumed that diffusion and kinetic impedances associated with Faradaic process were negligible because the electrodes were purged with argon prior to and during the impedance measurements. At high frequencies, a Warburg-like response was observed, corresponding to ion migration through the catalyst layer. The ionic resistance, R_{ionic}, can be obtained from the length of the Warburg-like region projected onto the real impedance (Z') axis (=R_{ionic}/3) [41]. Figure 3 shows the impedance spectra in the Nyquist plot at the open circuit voltage. The corresponding data are shown in Table 3. These data show that the ionic resistance

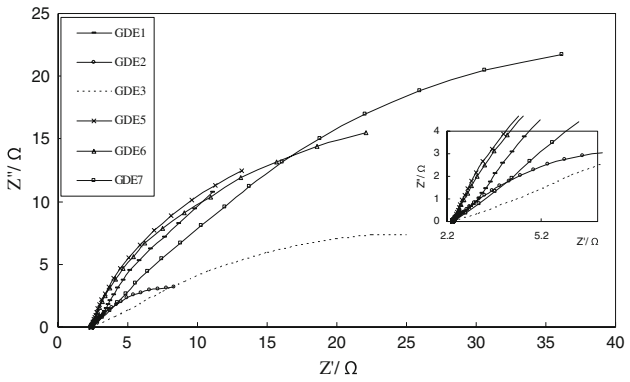

Fig. 3 Impedance data in the Nyquist representation obtained at open circuit voltage under oxygen reflux at 298 K. Inset: Zoom of the Nyquist diagram first points

Table 3 Ionic resistance of the tested electrodes extracted from Fig. 3

Number of GDEs	R_{ionic} (Ω)
GDE1	26
GDE2	19
GDE3	71
GDE4	90
GDE5	32
GDE6	60
GDE7	130
GDE8	42

in GDE2 is smaller than in the other GDEs, confirming the previous outcomes about this GDE. The data also shows that ionic resistances are higher in GDE6 and GDE7 than in the other GDEs. Ideally, it would be preferable to use Pt–Pd alloy in the catalyst layer.

3.5 Characterization of the alloy catalysts

Composition of the electrocatalysts was evaluated by ICP-AES analysis, and the results for compositions of all the catalysts were found to be near to the stoichiometric values. Figure 4 shows the X-ray diffraction patterns of the CNT-supported Pt alloy catalyst. The first peak located at ca. 26.5° in all the XRD patterns is associated with the CNT support. The other four peaks are characteristic of the face-centered-cubic (fcc) crystalline Pt (JCPDS-ICDD, Card No. 04-802), corresponding to the planes (1 1 1), (2 0 0), (2 2 0) and (3 1 1) at 2θ values of ca. 39.6°, 46.1°, 67.2° and 81.8°, respectively; indicating that all the alloy catalysts have principally single phase disordered structures (i.e. solid solutions). Since XRD is mass sensitive, a small

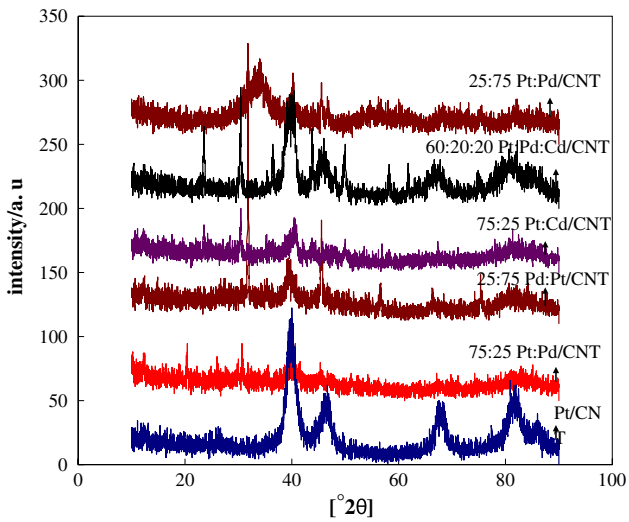

Fig. 4 XRD diffractograms of the CNT supported Pt and Pt alloy electrocatalysts

fraction of larger particles within the samples could produce the narrower diffraction peaks. Therefore, the broad diffraction peaks, as shown in Fig. 4, suggest that as-prepared 75:25 Pt–Pd/CNT and 75:25 Pt–Cd/CNT exist in small particles sizes with a relative narrow particle size distribution and in a disordered form. Further, as Fig. 4 shows, the PdO peak (JCPDS, Card No. 46-1211) for 25:75 Pd–Pt/CNT is very broad and its crystalline size is considered to be very small. Indeed, if the reflection intensities of the other metals are low compared with those of platinum and/or if the metals are present in amorphous compounds, they will not be detected in the diffractograms. A less likely possibility is that the nanotube contaminants, in the preparation procedure, were covered by platinum to the point of not being detected. The presence of palladium and cadmium, incorporated as a substitution in the platinum structure, was noted through the shift of the Bragg angles with respect to the values of the platinum. Compared to the same reflections in Pt, the diffraction peaks for the alloy catalysts were shifted very slightly to higher or lower 2θ values, probably indicating the formation of alloys involving Pd and Cd substituted into the fcc structure of the Pt. The crystallite size of the catalysts was estimated from the XRD data using the Debye-Scherrer equation. For this purpose, the (2 2 0) reflection of the Pt face centered cubic (fcc) structure around $2\theta = 67°$ was used. The particle size was calculated by the Debye-Scherrer equation [22]:

$$L = \frac{0.9\lambda_{\mathrm{Cu}K}}{B_{2\theta}\cos\theta_{\max}} \tag{7}$$

where, "L" is the average particle size; "$\lambda_{\mathrm{Cu}K}$" is the X-ray wavelength; "$B_{2\theta}$" is the full width at half maximum, and "$\theta_{\max}$" is the angle at peak maximum. The average particle sizes are provided in Table 4. For 75:25 Pt–Pd/CNT, the particle size was 29 nm, while for 60:20:20 Pt–Pd–Cd/CNT, it was significantly higher (43 nm). This large difference in particle size cannot be explained by the presence of other metals. Larger differences were also observed between 75:25 Pt–Pd/CNT and 50:50 Pt–Pd/CNT, and also between 75:25 Pt–Pd/CNT and 25:75 Pt–Pd/CNT. The crystallite size of 75:25 Pt–Pd/CNT supported on the nanotubes was 29 nm, while for 50:50 Pt–Pd/CNT and 25:75 Pt–Pd/CNT, it was much higher (57 and 58 nm, respectively). This reveals the effect of various amounts of Pt and Pd in the binary catalysts.

Table 4 Comparison of the average particle sizes from XRD

Number of GDEs	Average particles size from XRD (nm)
GDE1	46
GDE2	29
GDE3	58
GDE4	57
GDE6	35
GDE7	43
GDE8	29

4 Conclusions

The electrochemical properties of GDEs in acid medium, using Pt based binary and ternary alloy catalysts (prepared by the borohydride reduction processes) have been investigated. The results indicate that the amount of transition metals in catalysts may be one of the main factors in determining the performance of GDEs. Comparison of GDEs with Pt–Pd as catalyst, with different compositions of Pt and Pd in the catalyst layer, shows that GDE2 has the smallest Tafel slope. Impedance spectroscopy also shows that in GDE6 and GDE7 with Cd as transition metal, the ionic resistances are higher than in other GDEs. Further, GDE2 shows the smallest ionic resistance among other GDEs. Ideally, it would be preferable to use Pt–Pd alloy in the catalyst layer, because Pd forms less stable Pd–O bonds in GDE2 which is comparatively easier to reduce than Cd. It can be inferred that Cd will stabilize the Cd–O, resulting in a highly negative reduction potential, which is generally too negative to be of interest in power source applications.

XRD studies on these electrocatalysts suggested a change in crystallographic structure of the alloy electrocatalysts with respect to Pt.

The significantly lower costs of Pd and Cd catalysts and the relative abundance of these metals compared to Pt could enhance the commercial viability of fuel cell technology.

Our research indicates a promoting effect of the bimetallic catalyst in enhancing the ORR, and that Pt–Pd especially with 75:25 atomic ratio (used to prepare GDE2) could be an economical candidate to replace Pt as a cathode fuel-cell catalyst.

References

1. Golikand AN, Lohrasbi E, Maragheh MG et al (2008) J Appl Electrochem 38:869
2. Ralph TR, Hogarth MP (2002) Platin Met Rev 46(1):3
3. Larminie J, Dicks A (2000) Fuel cell systems explained. Wiley, Chichester
4. Freund A, Lang J, Lehmann T et al (1996) Catal Today 27:279
5. Lister S, McLean G (2004) J Power Sources 130:61
6. Stevens DA, Dahn JR (2003) J Electrochem Soc 6:A770
7. Arico AS, Srinivasan S, Antonucci V (2001) Fuel Cells 1(2):133
8. Ticianelli EA, Gonzalez ER (2003) In: Vielstich W, Gasteiger HA, Lamm A (eds) Handbook of fuel cells—fundamentals, technology and applications. Wiley, Chichester

9. Petrow HG, Allen RJ (1977) US Patent 4,044,193
10. Liu L, Pu C, Viswanathan R et al (1998) Electrochim Acta 43(24):3657
11. Winkler A, Guo X, Siddiqui HR et al (1988) Surf Sci 201:419
12. Murthi VS, Urian RC, Mukerjee S (2004) J Phys Chem B 108:11011
13. Stamenkovic VR, Schmidt TJ, Ross PN et al (2002) J Phys Chem B 106:11970
14. Paulus UA, Vokaun A, Scherer GG et al (2002) Electrochim Acta 47:3787
15. Paulus UA, Vokaun A, Scherer GG et al (2002) J Phys Chem B 106:4181
16. Mukerjee S, Srinivasan S, Soriaga MP (1995) J Phys Chem 99:4577
17. Fernandez JL, Walsh DA, Bard AJ (2005) J Am Chem Soc 127:357
18. Zhang J, Mo Y, Vukmirovic MB et al (2004) J Phys Chem B 108:10955
19. Balbuena PB, Altomare D, Agapito LA et al (2003) J Phys Chem B 107:13671
20. Wang Y, Balbuena PB (2005) J Phys Chem B 109:18902
21. Sidik RA, Anderson AB (2002) J Electroanal Chem 528:69
22. Karlberg GS (2006) Phys Rev B 74:153414
23. Shao MH, Huang T, Liu P et al (2006) Langmuir 22:10409
24. Zhang J, Vukmirovic MB, Xu Y et al (2005) Angew Chem Int Ed Engl 44:2132
25. Stamenkovic VR, Schmidt TJ, Ross PN et al (2003) J Electroanal Chem 554–555:191
26. Shao MH, Sasaki K, Adzic RR (2006) J Am Chem Soc 128:3526
27. Stamenkovic VR, Fowler B, Mun BS et al (2007) Science 315:493
28. Stamenkovic VR, Mun BS, Mayrhofer KJJ et al (2006) J Am Chem Soc 128:8813
29. Wang LL, Khare SV, Chirita V et al (2006) J Am Chem Soc 128:131
30. Calvo SR, Balbuena PB (2007) Surf Sci 601:165
31. Norskov JK, Rossmeisl J, Logadottir A et al (2004) J Phys Chem B 108:17886
32. Ishikawa Y, Mateo JJ, Tryk DA et al (2007) J Electroanal Chem 607:37
33. Pozio A, Francesco MD, Cemmi A et al (2002) J Power Sources 105:13
34. Perez J, Gonzalez ER, Ticianelli EA (1998) Electrochim Acta 44:1329
35. Ciureanu M, Wang H (1999) J Electrochem Soc 146:4031
36. Antolini E, Giorgi L, Pozio A et al (1999) J Power Sources 77:136
37. Sirinivasan S, Ticianelli EA, Derouin CR et al (1988) J Power Sources 22:359
38. Bard AJ, Parsons R (eds) (1985) Standard potentials in aqueous solutions. New York, Marcel Dekker
39. Bard AJ (ed) (1973) Encyclopedia of electrochemistry of the elements. New York, Marcel Dekker
40. Jiang H, Zhu L, Moon KS et al (2007) Carbon 45:655
41. Lefebvre MC, Martin RB, Pickup PG (1999) Electrochem Solid-State Lett 2:259